

# Band topology and dynamic multiferroicity induced from dynamical Dzyaloshinskii–Moriya interactions in centrosymmetric lattices

Bowen Ma<sup>1,2,\*</sup> and Z. D. Wang<sup>1,2,†</sup>

<sup>1</sup>*HK Institute of Quantum Science & Technology and Department of Physics,  
The University of Hong Kong, Pokfulam Road, Hong Kong, China*

<sup>2</sup>*Hong Kong Branch for Quantum Science Center of Guangdong-Hong  
Kong-Macau Great Bay Area, 3 Binlang Road, Shenzhen, China*

(Dated: May 13, 2025)

We develop a theory of a dynamical Dzyaloshinskii–Moriya interaction (dDMI) in centrosymmetric crystals by generally considering the vibration of both cations and anions. It gives rise to an antisymmetric spin-lattice coupling, inducing magnon-phonon hybridized topological excitations. Moreover, we find that this dDMI naturally exhibits a magnetoelectric feature, leading to the presence of dynamic multiferroicity with finite toroidal moment distribution in the momentum space. By comparing the toroidal moments with the band skyrmion structure, we reveal the intrinsic connection between band topology and dynamic multiferroicity through the dDMI.

**Introduction.**—The Dzyaloshinskii–Moriya interaction (DMI) is an antisymmetric exchange interaction between two localized spins. It was first proposed by Dzyaloshinskii [1] using Landau’s second-order phase transition theory to phenomenologically explain the origin of the weak ferromagnetism in the antiferromagnet  $\alpha$ -Fe<sub>2</sub>O<sub>3</sub>, where in contrast with the symmetric Heisenberg exchange interaction that favors spins to align collinearly, a different spin interaction tends to produce a spin canting from the perpendicular direction. Later, Moriya [2, 3] used a second-order perturbation analysis of the spin-orbit coupling (SOC) in Anderson’s superexchange model and derived the spin Hamiltonian of this interaction to be

$$H_{\text{DM}}^{ij} = \mathbf{D}_{ij} \cdot (\mathbf{S}_i \times \mathbf{S}_j) \quad (1)$$

for the coupling between  $\mathbf{S}_i$  and  $\mathbf{S}_j$  with  $\mathbf{D}_{ij} = -\mathbf{D}_{ji}$  now called Dzyaloshinskii–Moriya (DM) vector. In recent decades, DMI has been intensively studied for understanding various physical phenomena including spin-induced multiferroicity [4–9], non-reciprocal spin-wave propagation [10–13], magnon thermal Hall effects [14–16], spin torque and transport [17–22], and noncollinear spin textures such as chiral domain walls [23–26] and magnetic skyrmions [27–30].

In addition to SOC, the crystal symmetry has significant effects on inducing DMI. The orientation of the DM vector is restricted by the famous Moriya’s rule [3], especially the inversion symmetry within the bond  $ij$  needs to be broken for the presence of non-zero  $\mathbf{D}_{ij}$ . In centrosymmetric systems, by tuning the lattice deformation, strain engineering has been demonstrated as a controllable method to manipulate the DMI [31–33] and to achieve different spin textures such as magnetic skyrmions [34, 35]. While from a dynamical point of view, even without a static lattice distortion, the lattice vibration can “instantaneously” break the inversional symmetry. It is then natural to ask if the lattice dynamics along with the SOC can induce a DM-like spin-lattice coupling.

With these motivations, in the present Letter, we generally propose a dynamical DMI (dDMI) from lattice vibrations in a centrosymmetric lattice that couples spin degrees of freedom with lattice dynamics. Similar to the topological magnons induced from conventional static DMI [36–38], the excitation of this magnon-phonon coupled system develops non-trivial band topology. More remarkably, we notice the expression of the dDMI coincides with the spin-induced magnetoelectric effect in Katsura-Nagaosa-Balatsky (KNB) model [4, 6], giving rise to dynamic multiferroicity [39, 40]. By comparing the magnetoelectric toroidal moment [41–44] with the band skyrmion structure [45, 46] in the momentum space, we find the band topology and the dynamic multiferroicity are naturally connected by the dDMI.

**Dynamical DMI.**—We begin from a four-atom diamond cell as shown in Fig. 1(a), where magnetic ions reside at site  $\mathbf{R}_i$  and  $\mathbf{R}_j$  with spin  $\mathbf{S}_i$  and  $\mathbf{S}_j$  respectively, while non-magnetic ligands are located at  $\mathbf{R}_l$  and  $\mathbf{R}_m$ . Then, an out-of-plane DMI between  $\mathbf{S}_i$  and  $\mathbf{S}_j$  is allowed in principle, for example, in the (purple) triangular  $\Delta_{lj}$ , as

$$H_{\Delta_{lj}} = \mathbf{D}_{ilj} \cdot (\mathbf{S}_i \times \mathbf{S}_j), \quad \text{with } \mathbf{D}_{ilj} = D_{ij} \frac{\mathbf{R}_{li} \times \mathbf{R}_{lj}}{|\mathbf{R}_{li} \times \mathbf{R}_{lj}|}, \quad (2)$$

where  $\mathbf{R}_{li(j)} = \mathbf{R}_{i(j)} - \mathbf{R}_l$  is the distance vector of the bond  $i(j)l$ , and  $D_{ij}$  the coupling strength for the bond  $ij$ . The other (orange) triangle  $\Delta_{imj}$  also contributes a DMI  $\mathbf{D}_{imj}$  so that the total contribution is

$$H_D^0 = (\mathbf{D}_{ilj} + \mathbf{D}_{imj}) \cdot (\mathbf{S}_i \times \mathbf{S}_j). \quad (3)$$

Since this diamond structure is inversion symmetric at the bond- $ij$  center, according to Moriya’s rule,  $\mathbf{D}_{ilj}$  and  $\mathbf{D}_{imj}$  has the same coupling strength  $D_{ij}$  but opposite direction, and thus the total DMI is exactly zero. Now if we consider the lattice vibration at finite temperature as a dynamical distortion, the perfect cancellation of the DMI is expected to be violated [See Fig. 1(b)]. To illustrate this idea, we introduce a small displacement  $\mathbf{u}_{i(j)}$

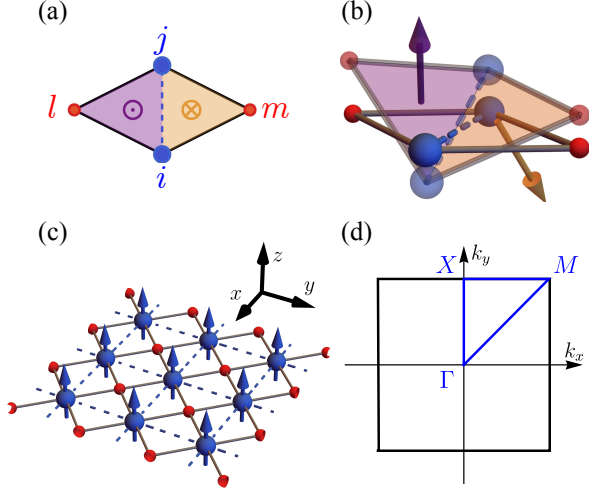


FIG. 1. (a) The static four-atom diamond cell with  $ij$  (blue) atoms magnetic but  $lm$  (red) atom non-magnetic. (b) The schematic for dynamical DMI. The purple and orange arrows indicate the DM vectors from purple and orange triangular respectively. (c) A ferromagnet in a diatomic square lattice, where blue (red) spheres stand for magnetic cations (non-magnetic anions). The blue arrows indicate magnetic moments along  $z$ -direction. (d) The Brillouin zone for the square lattice with a high-symmetry path  $\Gamma X M \Gamma$ .

of atoms  $i(j)$  and  $\mathbf{v}_{l(m)}$  of atoms  $l(m)$  away from their equilibrium position  $\mathbf{R}_{i(j)}^0$  and  $\mathbf{R}_{l(m)}^0$  respectively. After expanding the interaction Eq. 3 to the first order in  $\mathbf{u}$  and  $\mathbf{v}$ , we find a spin-lattice interaction as

$$H_{D,ij} = \frac{2D_0 \tan \frac{\theta}{2}}{a} \left[ \hat{\mathbf{R}}_{ij}^0 \times \hat{\mathbf{z}} (v_l^z + v_m^z - u_i^z - u_j^z) \right] \cdot (\mathbf{S}_i \times \mathbf{S}_j), \quad (4)$$

where  $D_0$  is the DMI from the triangle configuration in the equilibrium,  $a = |\mathbf{R}_{ij}^0|$  is the lattice constant,  $\theta$  is the angle between bond  $li$  and  $lj$  (or equivalently between bond  $mi$  and  $mj$ ) in the static limit, and  $\hat{\mathbf{z}}$  is the direction perpendicular to the diamond plane. Due to its antisymmetric form of the coupling, this spin-lattice interaction can be regarded as a dDMI that couples the collective modes of spin-waves and lattice vibrations. In previous studies on DMI-induced magnon-phonon coupling [47, 48], a non-zero DMI is needed by breaking the inversion symmetry from a heterostructure, and the strength of DMI needs to be small for not developing a spiral spin structure. However, in our case, the DMI is a dynamical one, which is originally hidden by the static symmetry, and thus will not undermine the classical magnetic order of the ground state.

*Square lattice example.*—We now apply the spin-lattice interaction Eq. 4 for the diamond cluster to a two-dimensional (2D) lattice system. In real materials, the ligands may not be perfectly located in the magnetic lattice plane and  $\hat{\mathbf{z}}$  for each diamond cluster can orient dif-

ferently. For example in  $\text{NiPS}_3$  and  $\text{CoTiO}_3$ , the magnetic moment does not align along the normal direction of the diamond cluster, but still have a non-zero component perpendicular to each diamond plane. Therefore, for simplicity but without loss of generality, we consider a toy model in a 2D square lattice as shown in Fig. 1(c), where the ligands are sitting at each square center and the magnetic configuration is an out-of-plane ferromagnetic order. The minimal spin Hamiltonian can be written as

$$H_s = -J \sum_{\langle ij \rangle} \mathbf{S}_i \cdot \mathbf{S}_j - \sum_i [\eta (\mathbf{S}_i^z)^2 + \mathcal{B} \mathbf{S}_i^z], \quad (5)$$

where  $J > 0$  is the nearest-neighbour ferromagnetic exchange coupling,  $\eta$  is the single-ion anisotropy and  $\mathcal{B}$  is the Zeeman splitting from the external magnetic field.

For this simple case, the effective dynamical DM vectors are in the plane and are all perpendicular to the collinear ferromagnetic order. Within the linear spin-wave regime, where the spin operators are represented by the creation and annihilation operators  $a^\dagger$  and  $a$  of Holstein-Primakoff magnons [49] as

$$\mathbf{S}_i^+ \approx \sqrt{2S} a_i, \quad \mathbf{S}_i^- \approx \sqrt{2S} a_i^\dagger, \quad \mathbf{S}_i^z = S - a_i^\dagger a_i, \quad (6)$$

this DMI will not affect the spin dynamics. Nevertheless, the DM-type spin-lattice interaction can hybridize magnons with the collective modes of the lattice vibration if they are energetically close to each other [50, 51]. These vibrational modes, i.e. phonons, can be described by the elastic Hamiltonian as

$$H_p = \sum_i \frac{P_i^2}{2M} + \sum_l \frac{p_l^2}{2m} + \frac{1}{2} k_u \sum_{\langle ij \rangle} (u_i^z - u_j^z)^2 + \frac{1}{2} k_{uv} \sum_{\langle il \rangle} (u_i^z - v_l^z)^2, \quad (7)$$

where  $P_i$  ( $p_l$ ) is the momentum of (non-)magnetic atom at site  $i$  ( $l$ ) with mass  $M$  ( $m$ ),  $k_{uv}$  ( $k_u$ ) is the first (second) nearest-neighbor bending constant. Here we ignore the elastic coupling between non-magnetic ligands as they are usually not chemically bonded.

The full Hamiltonian is then  $H = H_m + H_p + H_D$ , and it can be Fourier transformed into the momentum space as a generalized Bogoliubov-de-Gennes (BdG) Hamiltonian  $H = \frac{1}{2} \sum_{\mathbf{k}} \mathbf{X}_{\mathbf{k}}^\dagger H_{\mathbf{k}} \mathbf{X}_{\mathbf{k}}$  with  $\mathbf{X}_{\mathbf{k}} = (a_{\mathbf{k}}, a_{-\mathbf{k}}^\dagger, u_{\mathbf{k}}^z, v_{\mathbf{k}}^z, P_{-\mathbf{k}}, p_{-\mathbf{k}})^T$  and

$$H_{\mathbf{k}} = \begin{pmatrix} \varepsilon_{\mathbf{k}}^m I_2 & H_{mp}(\mathbf{k}) & 0 & 0 \\ H_{mp}^\dagger(\mathbf{k}) & \Phi(\mathbf{k}) & 0 & 0 \\ 0 & 0 & \frac{1}{M} & 0 \\ 0 & 0 & 0 & \frac{1}{m} \end{pmatrix}, \quad (8)$$

where  $\varepsilon_{\mathbf{k}}^m = 2JS[2 - \cos(k_x a) - \cos(k_y a)] + B_{\text{eff}}$  is the pure magnon dispersion from Eq. 5 with the effective

field  $B_{\text{eff}} = \mathcal{B} + (2S - 1)\eta$ ,  $I_n$  is the  $n \times n$  Identity matrix,  $\Phi(\mathbf{k})$  is the dynamical matrix of the vibration as

$$\begin{aligned} \Phi(\mathbf{k}) = & 4\tilde{M}\omega_{uv}^2 \begin{pmatrix} 1 & & -\cos \frac{k_x a}{2} \cos \frac{k_y a}{2} \\ -\cos \frac{k_x a}{2} \cos \frac{k_y a}{2} & & 1 \\ & & & \end{pmatrix} \\ & + 2M\omega_u^2 \begin{pmatrix} 2 - \cos(k_x a) - \cos(k_y a) & 0 \\ 0 & 0 \end{pmatrix} \end{aligned} \quad (9)$$

with  $\tilde{M} \equiv \frac{2mM}{m+M}$  as the reduced mass,  $\omega_{uv} = \sqrt{k_{uv}/\tilde{M}}$  and  $\omega_u = \sqrt{k_u/M}$  two intrinsic frequencies, and  $H_{mp}(\mathbf{k})$  is the magnon-phonon coupling from the effective DMI written explicitly as

$$\begin{aligned} H_{mp}(\mathbf{k}) = & \tilde{D} \begin{pmatrix} \sin k_y a & -2 \cos \frac{k_x a}{2} \sin \frac{k_y a}{2} \\ -\sin k_y a & 2 \cos \frac{k_x a}{2} \sin \frac{k_y a}{2} \end{pmatrix} \\ & + i\tilde{D} \begin{pmatrix} -\sin k_x a & 2 \sin \frac{k_x a}{2} \cos \frac{k_y a}{2} \\ -\sin k_x a & 2 \sin \frac{k_x a}{2} \cos \frac{k_y a}{2} \end{pmatrix}, \end{aligned} \quad (10)$$

with  $\tilde{D} = \frac{2D_0\sqrt{2S^3}}{a}$ .

For this basis  $\mathbf{X}_{\mathbf{k}}$ , the commutator relation can be expressed as

$$[\mathbf{X}_{\mathbf{k}}, \mathbf{X}_{\mathbf{k}}^\dagger] = \begin{pmatrix} 1 & 0 & 0 & 0 \\ 0 & -1 & 0 & 0 \\ 0 & 0 & 0 & iI_2 \\ 0 & 0 & -iI_2 & 0 \end{pmatrix} \equiv g, \quad (11)$$

and thus the  $n$ -th band dispersion  $E_{n\mathbf{k}}$  of the hybrid excitations  $|\psi_{n\mathbf{k}}\rangle$  can be calculated by the eigen-equation  $gH_{\mathbf{k}}|\psi_{n\mathbf{k}}\rangle = E_{n\mathbf{k}}|\psi_{n\mathbf{k}}\rangle$  [52]. We depict the band dispersion in the left column of Fig. 2 with  $J = 2$  meV,  $S = 1$  for typical 3d transition-metal compounds and take  $m/M = 1/3$  (e.g. O and S compared to Co and Ni approximately),  $\omega_{uv} = 8$  meV,  $\omega_u = 4$  meV. As the conventional DMI can be as large as 80% of the Heisenberg exchange  $J$  [53], we here set  $D_0 = 1$  meV. With an external magnetic field, the magnonic band can be energetically manipulated to couple with acoustic and/or optical phonons by tuning  $B_{\text{eff}}$ , and a gap opens up at those crossings between magnon and phonon bands. Because optical modes are out-of-phase movements of the atoms, they are more asymmetric than the acoustic modes, and thus they lead to a more prominent gap opening when hybridizing with magnons by the dDMI.

**Band topology.**—From the symmetry aspect, with the sine functions in  $H_{mp}$ , the effective DMI breaks the inversion symmetry, allowing non-trivial band topology. To show the topological effects of the DM-type spin-phonon coupling on the gap opening, we study the Berry curvature and band Chern numbers. For the BdG Hamiltonian, the Berry curvature [48, 54, 55] is defined as

$$\Omega_{n\mathbf{k}} = i\nabla_{\mathbf{k}} \times \langle \psi_{n\mathbf{k}} | g \nabla_{\mathbf{k}} | \psi_{n\mathbf{k}} \rangle, \quad (12)$$

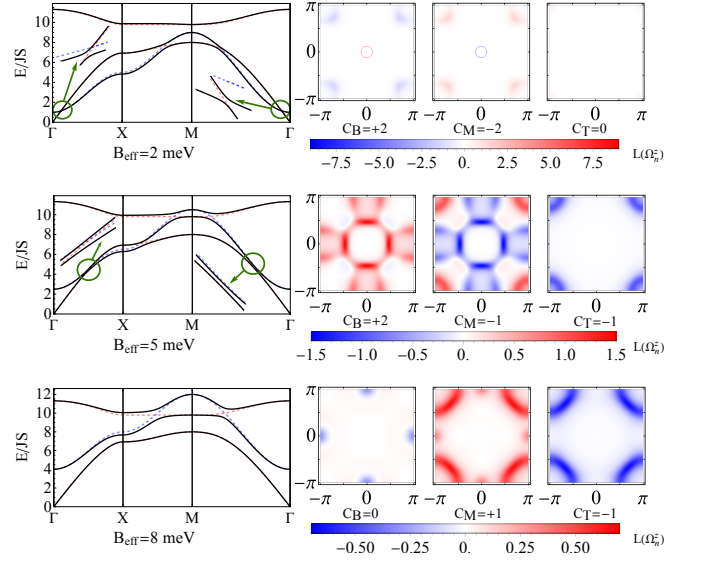


FIG. 2. Band dispersion and Berry curvature with  $J = 2$  meV,  $S = 1$ ,  $\omega_{uv} = 8$  meV,  $\omega_u = 4$  meV,  $m/M = 1/3$ ,  $D_0 = 1$  meV,  $B_{\text{eff}} = 2, 5,$  and  $8$  meV for the top, middle, and bottom panel, respectively.  $C_B, C_M,$  and  $C_T$  is the Chern number for the bottom, middle, and top band, respectively.

and the corresponding band Chern number is defined as the sum of the  $z$ -component  $\Omega_{n\mathbf{k}}^z$  over the first Brillouin zone [Fig. 1(d)],

$$C_n = \frac{1}{2\pi} \sum_{\mathbf{k}} \Omega_{n\mathbf{k}}^z. \quad (13)$$

In the right column of Fig. 2, we show the Berry curvature distribution in the momentum space and the Chern number for each band with different  $B_{\text{eff}}$ . It can be seen that large Berry curvature appears at those anti-crossing gaps where magnons and phonons are drastically hybridized by  $H_{mp}$ . The band Chern numbers can be changed by moving the magnon band with an external magnetic field, which provides experimental tunability.

As a powerful probe for detecting the topology of charge-neutral excitations, in our model Hamiltonian with the dDMI, we study the thermal Hall effects [56–60], where the thermal Hall conductivity is evaluated as [57, 61]

$$\kappa_{yx} = \frac{k_B^2 T}{\hbar V} \sum_{n,\mathbf{k}} \left[ c_2(g(E_{n\mathbf{k}}, T)) - \frac{\pi^2}{3} \right] \Omega_{n\mathbf{k}}^z, \quad (14)$$

with  $c_2(x) = (1+x)\ln^2(1+1/x) - \ln^2 x - 2\text{Li}_2(-x)$ ,  $\text{Li}_2(x)$  is the polylogarithm function,  $T$  is the average temperature,  $V$  is the system volume. We estimate the Curie temperature is about  $\frac{2}{3}S(S+1)zJ \sim 60$  K, and evaluate the thermal Hall conductivity up to 40 K in Fig. 3 with varying magnetic fields. The two vertical dashed lines represent the gap closing points separating the three topological phases in Fig. 2, and the trend of the

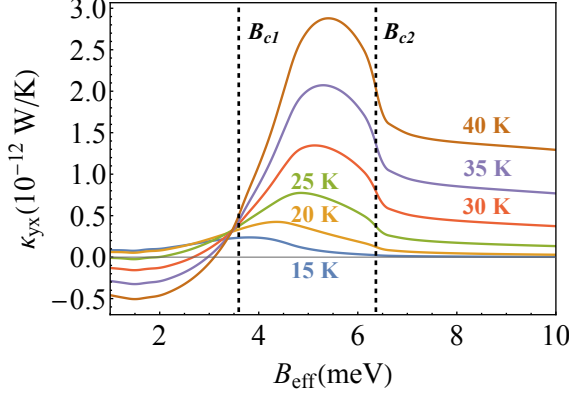


FIG. 3. The dependence of thermal Hall effects on  $B_{\text{eff}}$  for  $T = 15$  K, 20 K, 25 K, 30 K, 35 K, and 40 K, respectively. The topological gap in Fig. 2 closes at  $B_{c1} \approx 3.60$  meV or  $B_{c2} \approx 6.37$  meV.

curves clearly reflects these topological phase transitions under the effective magnetic field  $B_{\text{eff}}$ .

*Dynamic multiferroicity.*—Interestingly, although we derive Eq. 4 from a magnetoelastic consideration, the expression of the dDMI exhibits a magnetoelectric nature. This is because the electrical polarization in (ionic) crystals is associated with the vibration of charged ions. For example, in our diatomic model, the cations and the anions are supposed to have opposite effective charges  $\pm Q^*$ , and the vibration in the diamond  $ilmj$  provides an electric polarization  $\mathbf{P}_{ilmj} \sim Q^*(u_i^z + u_j^z - v_l^z - v_m^z)\hat{\mathbf{z}}$  along  $z$ -direction. Therefore, the electric polarization  $\mathbf{P}_{ilmj}$  and the magnetization  $\mathbf{M}_{ij}$  from the spin  $\mathbf{S}_i$  and  $\mathbf{S}_j$  are coupled by the dDMI.

More remarkably, we can rewrite Eq. 4 as

$$H_{D,ij} = \frac{2D_0 \tan \frac{\theta}{2}}{a} (u_i^z + u_j^z - v_l^z - v_m^z)\hat{\mathbf{z}} \cdot [\hat{\mathbf{R}}_{ij}^0 \times (\mathbf{S}_i \times \mathbf{S}_j)]. \quad (15)$$

According to the KNB mechanism [4],  $\hat{\mathbf{R}}_{ij}^0 \times (\mathbf{S}_i \times \mathbf{S}_j)$  is proportional to an electrical polarization  $\mathbf{P}_{ij}^s$  produced between  $\mathbf{S}_i$  and  $\mathbf{S}_j$ . Then, the magnetoelectric entanglement of this dDMI can be understood in the spin-wave propagation picture [6, 62], where the precession of the spins induces a varying  $\mathbf{P}_{ij}^s$  with an alternating electrical field so that  $\mathbf{P}_{ilmj}$  is coupled with the spin dynamics. Consequently, despite the fact that the system is not ferroelectric as static polarization  $\langle \mathbf{P}_{ilmj} \rangle = 0$ , given that the fluctuation of the ferroelectric and the ferromagnetic degrees of freedom coexist and are entangled, this dDMI, as a magnetoelectric effect, will lead to the presence of dynamic multiferroicity.

Since the band topology results from dDMI, the topological excitations should naturally possess multiferroic features. In the literature, to characterize multiferroicity, the cross product of polarization  $\mathbf{P}$  and magnetization  $\mathbf{M}$

called the toroidal moment  $\mathbf{T} = \mathbf{P} \times \mathbf{M}$  has been introduced. In our case, a dynamical toroidal moment can be defined as,

$$\begin{aligned} \mathbf{T} &= \sum_i \left[ Q^*(u_i^z - \frac{1}{4} \sum_{l \in n.n.} v_l^z)\hat{\mathbf{z}} \times \gamma \hbar \mathbf{S}_i \right] \equiv \sum_{\mathbf{k}} \mathbf{T}_{\mathbf{k}} \\ &\approx \hbar \gamma Q^* \sqrt{\frac{S}{2}} \sum_{\mathbf{k}} \left( u_{\mathbf{k}}^z - v_{\mathbf{k}}^z \cos \frac{k_x a}{2} \cos \frac{k_y a}{2} \right) \\ &\quad \times \left[ i(a_{-\mathbf{k}} - a_{\mathbf{k}}^\dagger)\hat{\mathbf{x}} + (a_{-\mathbf{k}} + a_{\mathbf{k}}^\dagger)\hat{\mathbf{y}} \right] \end{aligned} \quad (16)$$

with  $\gamma$  the gyromagnetic ratio, and  $\mathbf{T}_{\mathbf{k}}$  the momentum-resolved toroidal moment.

As the effects of dDMI is more significant when magnons couple with optical phonons, we investigate the case with  $B_{\text{eff}} = 8$  meV as an example, where the acoustic phonon is energetically well-separated from the other two bands. In Fig. 4(a) and (b), the finite and zero toroidal moment  $\langle \psi_{2,\mathbf{k}} | \mathbf{T}_{\mathbf{k}} | \psi_{2,\mathbf{k}} \rangle$  for  $D_0 \neq 0$  and  $D_0 = 0$  indicate the dDMI is significant for inducing dynamic multiferroicity. Since the acoustic phonon can be safely neglected from a perturbative point of view, to understand the relation between dDMI-induced band topology and the corresponding dynamic multiferroicity, we focus on the effective optical phonon-magnon Hamiltonian written in the Pauli matrices  $\boldsymbol{\sigma} = (\sigma_x, \sigma_y, \sigma_z)$  as

$$\tilde{H}_{\mathbf{k}} = \frac{1}{2}(\varepsilon_{\mathbf{k}}^m + \varepsilon_{\mathbf{k}}^+)I_2 + \mathbf{d}_{\mathbf{k}} \cdot \boldsymbol{\sigma} + \mathcal{V}_{\mathbf{k}} \quad (17)$$

with

$$\begin{cases} d_{\mathbf{k}}^x = -\frac{2\tilde{D} \sin \frac{k_y a}{2}}{\sqrt{2m\varepsilon_{\mathbf{k}}^+}} \left( \lambda \cos \frac{k_y a}{2} \sin \theta_{\mathbf{k}} + \cos \frac{k_x a}{2} \cos \theta_{\mathbf{k}} \right), \\ d_{\mathbf{k}}^y = -\frac{2\tilde{D} \sin \frac{k_x a}{2}}{\sqrt{2m\varepsilon_{\mathbf{k}}^+}} \left( \lambda \cos \frac{k_x a}{2} \sin \theta_{\mathbf{k}} + \cos \frac{k_y a}{2} \cos \theta_{\mathbf{k}} \right), \\ d_{\mathbf{k}}^z = \frac{1}{2}(\varepsilon_{\mathbf{k}}^m - \varepsilon_{\mathbf{k}}^o), \end{cases} \quad (18)$$

where  $\lambda = \sqrt{m/M}$ ,  $\varepsilon_{\mathbf{k}}^{m(o)}$  is the dispersion of magnons (optical phonons) when  $\tilde{D} = 0$ ,  $\tan 2\theta_{\mathbf{k}} = \frac{8\lambda\omega_{uv}^2 \cos \frac{k_x a}{2} \cos \frac{k_y a}{2}}{4(1-\lambda^2)\omega_{uv}^2 + (1+\lambda^2)(\cos k_x a + \cos k_y a - 2)\omega_u^2}$ , and  $\mathcal{V}_{\mathbf{k}}$  is a perturbation that does not contribute to the gap opening and we thus ignore it in the following. The derivation details can be found in the supplement. Then, the two eigenstates of  $\tilde{H}_{\mathbf{k}}$  can be analytically obtained as  $|\psi_{\mathbf{k}}^\pm\rangle = \frac{1}{\sqrt{2|\mathbf{d}_{\mathbf{k}}|(|\mathbf{d}_{\mathbf{k}}| \pm d_z^z)}} (d_z^z \pm |\mathbf{d}_{\mathbf{k}}|, d_{\mathbf{k}}^x + id_{\mathbf{k}}^y)^T$  for the upper and lower band respectively, and the corresponding toroidal moment for these two states  $\langle \mathbf{T}_{\mathbf{k}} \rangle_{\pm} = \langle \psi_{\mathbf{k}}^\pm | \mathbf{T}_{\mathbf{k}} | \psi_{\mathbf{k}}^\pm \rangle$  is proportional to  $\mathbf{d}$ -vector as,

$$\langle \mathbf{T}_{\mathbf{k}} \rangle_{\pm} = \mp C_{\mathbf{k}} \left( \hat{d}_{\mathbf{k}}^y \hat{\mathbf{x}} + \hat{d}_{\mathbf{k}}^x \hat{\mathbf{y}} \right), \quad (19)$$

where  $C_{\mathbf{k}} = \hbar \gamma Q^* \sqrt{\frac{S}{2}} \left( \frac{\sin \theta_{\mathbf{k}}}{\sqrt{2M\varepsilon_{\mathbf{k}}^+}} + \frac{\cos \theta_{\mathbf{k}} \cos \frac{k_x a}{2} \cos \frac{k_y a}{2}}{\sqrt{2m\varepsilon_{\mathbf{k}}^+}} \right)$ , and  $\hat{d}_{\mathbf{k}}^\alpha = d_{\mathbf{k}}^\alpha / |\mathbf{d}_{\mathbf{k}}|$  for  $\alpha = x, y, z$ .

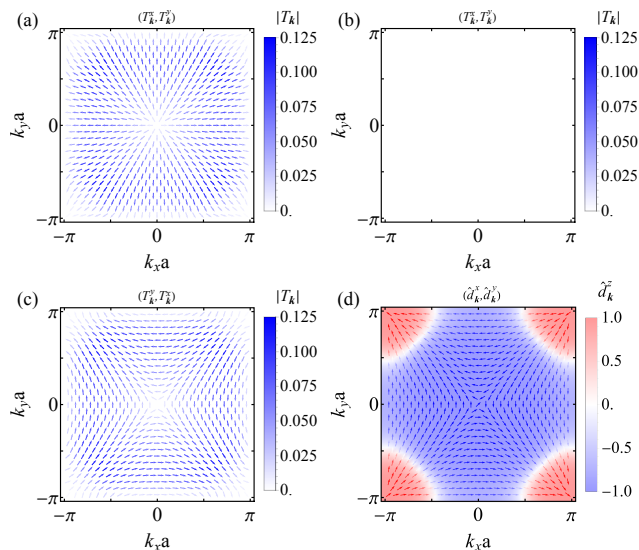


FIG. 4. (a) Non-zero toroidal moment distribution for the middle band for  $B_{\text{eff}} = 8$  meV when  $D_0 \neq 0$ , characterizing dynamic multiferroicity. (b) Toroidal moments become zero everywhere in the momentum space when  $D_0 = 0$ . (c) The rotated toroidal moment  $(T_{\mathbf{k}}^x, T_{\mathbf{k}}^y)$ , which is approximately proportional to  $(\hat{d}_{\mathbf{k}}^x, \hat{d}_{\mathbf{k}}^y)$  as shown in Fig. 4(d). (d) The skyrmion structure of the  $\mathbf{d}$ -vector for the effective magnon-phonon Hamiltonian.

On the other hand, the orientation of  $\mathbf{d}$ -vector over the  $\mathbf{k}$ -space reflects the topological property of the gap [45, 46, 63]. In Fig. 4, we plot the unit vector  $\hat{\mathbf{d}}_{\mathbf{k}}$  in the momentum space, which exhibits a Neel-type skyrmion structure centered at  $\mathbf{M}$  with a skyrmion number  $Q_{\text{skyrmion}} = +1$ . This is reminiscent of the winding number of  $\mathbf{d}$ -vector over the unit sphere in  $\mathbf{k}$ -space, and gives rise to the topological invariant Chern number  $+Q_{\text{skyrmion}}(-Q_{\text{skyrmion}})$  for the lower (upper) band as the Berry curvature for  $|\psi_{\mathbf{k}}^{\pm}\rangle$  is  $\Omega_{\mathbf{k}}^{\pm} = \pm \frac{1}{2} \hat{\mathbf{d}}_{\mathbf{k}} \cdot (\partial_{k_x} \hat{\mathbf{d}}_{\mathbf{k}} \times \partial_{k_y} \hat{\mathbf{d}}_{\mathbf{k}})$ . Since  $\hat{d}_{\mathbf{k}}^x, \hat{d}_{\mathbf{k}}^y \propto \tilde{D}$ , we find that the dDMI naturally connects hybridized band topology with dynamic multiferroicity characterized by the toroidal magnetoelectric moment.

*Discussions.*—In this work, we used a ferromagnetic configuration as a proof of principle, but we emphasize that in the derivation of Eq. 4 there is no restriction on spin orientation, and thus our model can be generally applied to ferri-, antiferro-magnetic order or non-collinear spin textures as well. In particular, as antiferromagnets can host ultrafast spin dynamics in the terahertz frequency region [64, 65], we expect a more predominant effect from dDMI on the coupling between optical phonons and antiferromagnetic magnons. Moreover, the  $l$ -atom and  $m$ -atom actually are not required to be non-magnetic, which further enhance the general applicability of our proposed dDMI in a variety of magnetic materials.

Besides, the magnetoelectric nature of the dDMI sug-

gests its possible application on multiferroic materials. One example is the 2D van der Waals multiferroic  $\text{NiI}_2$  [66, 67], which was recently suggested to be a type-II multiferroic material with a helimagnetic ground state. The conventional DMI is not allowed by the inversion symmetry [68], but it is interesting to consider the interplay between phonons and the helical order via the dDMI as well as the topology of their hybridization, which may provide electrical [69–71] or optical [72] approaches to exciting or detecting topological excitations.

As the thermal Hall signal induced from our model is comparable to the result from the magnetoelastic model [73, 74], by including the vibrational degrees of freedom of the non-magnetic atoms and the coupling between magnons and optical phonons, we expect our model to be complementary to other mechanisms and may explain the experimental observation for the high-temperature regime in centrosymmetric magnets, such as  $\text{FeCl}_2$  [75]. Given that the dDMI induces both finite Berry curvature and non-zero toroidal moments, similar to spin Nernst effects [76–79], transverse thermal transport of toroidal moments is expected to occur, which we leave for future study.

In summary, we have proposed an unconventional dynamical DMI in centrosymmetric crystals by considering the lattice vibrations of both magnetic and non-magnetic atoms. It can hybridize magnon excitations with lattice dynamics and induce non-trivial band topology. More importantly, we remark on the intrinsic magnetoelectric feature of this dynamical DMI and introduce dynamic multiferroicity via the well-known KNB model. By investigating the toroidal moment distribution and skyrmion structure in the momentum space, we further uncover that band topology and dynamic multiferroicity are essentially connected through dynamical DMI. We envision this study offers a new way for inducing and tuning topological excitations in various magnetic materials without inversion symmetry breaking, and suggests broad applications in spintronics, multiferroics, electromagnonics [80], and magnetophononics [81].

*Acknowledgment.*—We thank Ji Zou, Jeongheon Choe, and Anyuan Gao for useful discussions, Gang Chen for inspiring references, and Gregory Fiete for constructive comments on the manuscript. This work is supported by the Collaborative Research Fund of Hong Kong with Grant No. C7012-21G, by the NSFC/RGC JRS grant with Grant No. N\_HKU774/21, by the General Research Fund of Hong Kong with Grants No. 17310622 and No. 17303023.

\* bowenphy@hku.hk

† zwang@hku.hk

[1] I. Dzyaloshinsky, Journal of physics and chemistry of

- solids **4**, 241 (1958).
- [2] T. Moriya, Phys. Rev. Lett. **4**, 228 (1960).
  - [3] T. Moriya, Phys. Rev. **120**, 91 (1960).
  - [4] H. Katsura, N. Nagaosa, and A. V. Balatsky, Phys. Rev. Lett. **95**, 057205 (2005).
  - [5] M. Mostovoy, Phys. Rev. Lett. **96**, 067601 (2006).
  - [6] H. Katsura, A. V. Balatsky, and N. Nagaosa, Phys. Rev. Lett. **98**, 027203 (2007).
  - [7] I. A. Sergienko and E. Dagotto, Phys. Rev. B **73**, 094434 (2006).
  - [8] T. Kimura, T. Goto, H. Shintani, K. Ishizaka, T.-h. Arima, and Y. Tokura, nature **426**, 55 (2003).
  - [9] S. Ishiwata, Y. Taguchi, H. Murakawa, Y. Onose, and Y. Tokura, science **319**, 1643 (2008).
  - [10] K. Zakari, Y. Zhang, J. Prokop, T.-H. Chuang, N. Sakr, W. X. Tang, and J. Kirschner, Phys. Rev. Lett. **104**, 137203 (2010).
  - [11] L. Udvardi and L. Szunyogh, Phys. Rev. Lett. **102**, 207204 (2009).
  - [12] J.-H. Moon, S.-M. Seo, K.-J. Lee, K.-W. Kim, J. Ryu, H.-W. Lee, R. D. McMichael, and M. D. Stiles, Phys. Rev. B **88**, 184404 (2013).
  - [13] R. Zivieri, A. Giordano, R. Verba, B. Azzerboni, M. Carpentieri, A. N. Slavin, and G. Finocchio, Phys. Rev. B **97**, 134416 (2018).
  - [14] Y. Onose, T. Ideue, H. Katsura, Y. Shiomi, N. Nagaosa, and Y. Tokura, Science **329**, 297 (2010).
  - [15] P. Laurell and G. A. Fiete, Phys. Rev. B **98**, 094419 (2018).
  - [16] K. Hwang, N. Trivedi, and M. Randeria, Phys. Rev. Lett. **125**, 047203 (2020).
  - [17] A. Manchon, P. B. Ndiaye, J.-H. Moon, H.-W. Lee, and K.-J. Lee, Phys. Rev. B **90**, 224403 (2014).
  - [18] A. A. Kovalev and V. Zyuzin, Phys. Rev. B **93**, 161106 (2016).
  - [19] B. Ma, B. Flebus, and G. A. Fiete, Phys. Rev. B **101**, 035104 (2020).
  - [20] W. Lin, J. He, B. Ma, M. Matzelle, J. Xu, J. Freeland, Y. Choi, D. Haskel, B. Barbiellini, A. Bansil, *et al.*, Nature Physics **18**, 800 (2022).
  - [21] D. Yu, Y. Ga, J. Liang, C. Jia, and H. Yang, Phys. Rev. Lett. **130**, 056701 (2023).
  - [22] X. Ye, Q. Cui, W. Lin, and T. Yu, Phys. Rev. B **111**, 064401 (2025).
  - [23] M. Heide, G. Bihlmayer, and S. Blügel, Phys. Rev. B **78**, 140403 (2008).
  - [24] A. Thiaville, S. Rohart, É. Jué, V. Cros, and A. Fert, Europhysics Letters **100**, 57002 (2012).
  - [25] K.-S. Ryu, L. Thomas, S.-H. Yang, and S. Parkin, Nature nanotechnology **8**, 527 (2013).
  - [26] J. Sampaio, V. Cros, S. Rohart, A. Thiaville, and A. Fert, Nature nanotechnology **8**, 839 (2013).
  - [27] S. M<sup>u</sup>hlbauer, B. Binz, F. Jonietz, C. Pfleiderer, A. Rosch, A. Neubauer, R. Georgii, and P. B<sup>o</sup>ni, Science **323**, 915 (2009).
  - [28] X. Yu, Y. Onose, N. Kanazawa, J. H. Park, J. Han, Y. Matsui, N. Nagaosa, and Y. Tokura, Nature **465**, 901 (2010).
  - [29] W. Jiang, P. Upadhyaya, W. Zhang, G. Yu, M. B. Jungfleisch, F. Y. Fradin, J. E. Pearson, Y. Tserkovnyak, K. L. Wang, O. Heinonen, *et al.*, Science **349**, 283 (2015).
  - [30] A. Fert, N. Reyren, and V. Cros, Nature Reviews Materials **2**, 1 (2017).
  - [31] D. A. Kitchaev, I. J. Beyerlein, and A. Van der Ven, Phys. Rev. B **98**, 214414 (2018).
  - [32] A. V. Davydenko, A. G. Kozlov, A. G. Kolesnikov, M. E. Stebliy, G. S. Suslin, Y. E. Vekovshinin, A. V. Sadovnikov, and S. A. Nikitov, Phys. Rev. B **99**, 014433 (2019).
  - [33] W. Zhang, R. Chen, B. Jiang, X. Zhao, W. Zhao, S. Yan, G. Han, S. Yu, G. Liu, and S. Kang, Nanoscale **13**, 2665 (2021).
  - [34] Y. Zhang, J. Liu, Y. Dong, S. Wu, J. Zhang, J. Wang, J. Lu, A. Rückriegel, H. Wang, R. Duine, H. Yu, Z. Luo, K. Shen, and J. Zhang, Phys. Rev. Lett. **127**, 117204 (2021).
  - [35] Z. Shen, C. Song, Y. Xue, Z. Wu, J. Wang, and Z. Zhong, Phys. Rev. B **106**, 094403 (2022).
  - [36] S. Owerre, Journal of Applied Physics **120** (2016).
  - [37] S. K. Kim, H. Ochoa, R. Zarzuela, and Y. Tserkovnyak, Phys. Rev. Lett. **117**, 227201 (2016).
  - [38] P. A. McClarty, Annual Review of Condensed Matter Physics **13**, 171 (2022).
  - [39] D. M. Juraschek, M. Fechner, A. V. Balatsky, and N. A. Spaldin, Phys. Rev. Mater. **1**, 014401 (2017).
  - [40] K. Dunnett, J.-X. Zhu, N. A. Spaldin, V. Juričić, and A. V. Balatsky, Phys. Rev. Lett. **122**, 057208 (2019).
  - [41] V. Dubovik and V. Tugushev, Physics reports **187**, 145 (1990).
  - [42] M. Fiebig, Journal of physics D: applied physics **38**, R123 (2005).
  - [43] N. A. Spaldin, M. Fiebig, and M. Mostovoy, Journal of Physics: Condensed Matter **20**, 434203 (2008).
  - [44] C. Ederer and N. A. Spaldin, Phys. Rev. B **76**, 214404 (2007).
  - [45] X.-L. Qi, T. L. Hughes, and S.-C. Zhang, Phys. Rev. B **78**, 195424 (2008).
  - [46] X.-L. Qi and S.-C. Zhang, Rev. Mod. Phys. **83**, 1057 (2011).
  - [47] X. Zhang, Y. Zhang, S. Okamoto, and D. Xiao, Phys. Rev. Lett. **123**, 167202 (2019).
  - [48] B. Ma and G. A. Fiete, Phys. Rev. B **105**, L100402 (2022).
  - [49] T. Holstein and H. Primakoff, Phys. Rev. **58**, 1098 (1940).
  - [50] J. Jensen, Intern. J. Magn. **1**, 271 (1971).
  - [51] D. T. Vigen and S. H. Liu, Phys. Rev. B **5**, 2719 (1972).
  - [52] B. Ma, Z. D. Wang, and G. v. Chen, Phys. Rev. Lett. **133**, 246604 (2024).
  - [53] S. Zhang, X. Li, H. Zhang, P. Cui, X. Xu, and Z. Zhang, npj Quantum Materials **8**, 38 (2023).
  - [54] M. V. Berry, Proceedings of the Royal Society of London. A. Mathematical and Physical Sciences **392**, 45 (1984).
  - [55] R. Takahashi and N. Nagaosa, Phys. Rev. Lett. **117**, 217205 (2016).
  - [56] C. Strohm, G. L. J. A. Rikken, and P. Wyder, Phys. Rev. Lett. **95**, 155901 (2005).
  - [57] R. Matsumoto and S. Murakami, Phys. Rev. Lett. **106**, 197202 (2011).
  - [58] K. Sugii, M. Shimozawa, D. Watanabe, Y. Suzuki, M. Halim, M. Kimata, Y. Matsumoto, S. Nakatsuji, and M. Yamashita, Phys. Rev. Lett. **118**, 145902 (2017).
  - [59] G. Grissonnanche, S. Thériault, A. Gourgout, M.-E. Boulanger, E. Lefrançois, A. Ataie, F. Laliberté, M. Dion, J.-S. Zhou, S. Pyon, *et al.*, Nature Physics **16**, 1108 (2020).
  - [60] X.-T. Zhang, Y. H. Gao, and G. Chen, Physics Reports

- 1070**, 1 (2024).
- [61] R. Matsumoto and S. Murakami, Phys. Rev. B **84**, 184406 (2011).
- [62] D. Khomskii, Physics **2**, 20 (2009).
- [63] B. A. Bernevig, Topological insulators and topological superconductors (Princeton university press, 2013) p. 9.
- [64] O. Gomonay, V. Baltz, A. Brataas, and Y. Tserkovnyak, Nature Physics **14**, 213 (2018).
- [65] V. Baltz, A. Manchon, M. Tsoi, T. Moriyama, T. Ono, and Y. Tserkovnyak, Rev. Mod. Phys. **90**, 015005 (2018).
- [66] H. Ju, Y. Lee, K.-T. Kim, I. H. Choi, C. J. Roh, S. Son, P. Park, J. H. Kim, T. S. Jung, J. H. Kim, *et al.*, Nano letters **21**, 5126 (2021).
- [67] Q. Song, C. A. Occhialini, E. Ergeçen, B. Ilyas, D. Amoroso, P. Barone, J. Kapteghian, K. Watanabe, T. Taniguchi, A. S. Botana, *et al.*, Nature **602**, 601 (2022).
- [68] X. Li, C. Xu, B. Liu, X. Li, L. Bellaiche, and H. Xiang, Phys. Rev. Lett. **131**, 036701 (2023).
- [69] K. Shen, Phys. Rev. B **108**, 094413 (2023).
- [70] R. R. Neumann, J. Henk, I. Mertig, and A. Mook, Phys. Rev. B **109**, L180412 (2024).
- [71] K. Li, L. Wang, Y. Wang, Y. Guo, S. Lv, Y. He, W. Lin, T. Min, S. Hu, S. Yang, *et al.*, Advanced Materials **36**, 2312137 (2024).
- [72] S. Miyahara and N. Furukawa, Journal of the Physical Society of Japan **81**, 023712 (2012).
- [73] G. Go, S. K. Kim, and K.-J. Lee, Phys. Rev. Lett. **123**, 237207 (2019).
- [74] S. Zhang, G. Go, K.-J. Lee, and S. K. Kim, Physical Review Letters **124**, 147204 (2020).
- [75] C. Xu, C. Carnahan, H. Zhang, M. Sretenovic, P. Zhang, D. Xiao, and X. Ke, Phys. Rev. B **107**, L060404 (2023).
- [76] V. A. Zyuzin and A. A. Kovalev, Physical Review Letters **117**, 217203 (2016).
- [77] R. Cheng, S. Okamoto, and D. Xiao, Physical Review Letters **117**, 217202 (2016).
- [78] B. Li, S. Sandhoefner, and A. A. Kovalev, Phys. Rev. Res. **2**, 013079 (2020).
- [79] B. Ma and G. A. Fiete, Physical Review B **104**, 174410 (2021).
- [80] J. Xu, C. Zhong, X. Han, D. Jin, L. Jiang, and X. Zhang, Phys. Rev. Lett. **125**, 237201 (2020).
- [81] M. Fechner, A. Sukhov, L. Chotorlishvili, C. Kenel, J. Berakdar, and N. A. Spaldin, Phys. Rev. Mater. **2**, 064401 (2018).